ECCOMAS Congress 2016
VII European Congress on Computational Methods in Applied Sciences and Engineering
M. Papadrakakis, V. Papadopoulos, G. Stefanou, V. Plevris (eds.)
Crete Island, Greece, 5–10 June 2016

NONLINEAR DYNAMIC BEHAVIOUR OF BASE-ISOLATED BUILDINGS WITH THE FRICTION PENDULUM SYSTEM SUBJECTED TO NEAR-FAULT EARTHQUAKES

F. Mazza[1] **and S. Sisinno**[2]

[1]Dipartimento di Ingegneria Civile, Università della Calabria
Via P. Bucci, 87036 Rende (CS), Italy
fabio.mazza@unical.it

[2]Dipartimento di Ingegneria Civile, Università della Calabria
Via P. Bucci, 87036 Rende (CS), Italy
sandro_sisinno@libero.it

Keywords: R.c. base-isolated structures, Friction pendulum system, Torsional effect, Residual displacement, Uplift, Near-fault earthquakes, Nonlinear dynamic analysis.

Abstract. *In spite of the fact that avant-garde sliding bearings have been proposed, the application of the single friction pendulum (FP) bearing is increasing due to its conceptual simplicity; yet there are still important aspects of its behaviour that need further attention. More specifically, the FP system presents spatial variation of friction coefficient, depending on the sliding velocity of the FP bearings. Moreover, the frictional force and restoring stiffness during the sliding phase are proportional to the axial load. Long duration intense velocity pulses in the horizontal direction and high values of the ratio between vertical and horizontal peak ground acceleration are expected for near-fault earthquakes. Torsion with residual displacement and uplift of the FP system need to be better understood for base-isolated structures located in near-fault areas. To this end, a numerical investigation is carried out with reference to a six-storey reinforced concrete (r.c.) framed building, characterized by an L-shaped plan with wings of different length and setbacks at different heights along the main in-plan directions. Twelve base-isolated test structures are designed in line with the Italian seismic code, considering (besides the gravity loads) the horizontal seismic loads acting alone or in combination with the vertical ones. Three design values of the radius of curvature for the FP system and two in-plan distributions of dynamic-fast friction coefficient for the FP bearings, ranging from a constant value for all isolators to a different value for each, are assumed. A nonlinear force-displacement law of the FP bearings in the horizontal direction, depending on sliding velocity and axial load, is considered, while a gap model takes into account the vertical uplift of the FP bearings. The nonlinear seismic analysis is performed on two sets of seven near-fault earthquakes, both sets with significant horizontal or vertical components selected and normalized on the basis of the design hypotheses adopted for the test structure.*

1 INTRODUCTION

The friction pendulum (FP) system is one of the most in-demand techniques for the seismic isolation of buildings [1], where the geometry and gravity allow a minimization of torsion and a self-centring of the base-isolation FP system for a wide range of frequency inputs [2]. However, the (low) constant isolation frequency, proportional to the curvature of the sliding surface, may induce resonance of base-isolated structures if it is close to the predominant vibration period of near-fault ground motions [3]. Specifically, fling-step and forward-directivity in near-fault areas can produce long duration pulses of intense velocity in the horizontal direction [4, 5], amplifying the displacement and inducing torsional and re-centring problems [6, 7]. On the other hand, since the response of the FP system during the sliding phase is strongly influenced by the axial load, amplification of torsional demand and residual displacement and uplift of the FP bearings may also be induced by the high frequency vertical component of near-fault earthquakes [8-10]. This vertical motion is characterized by peak ground acceleration higher than the horizontal one and closer in time for decreasing values of distance from the fault [11, 12].

In order to verify the occurrence of torsion with residual displacement and uplift of the FP system for base-isolation of structures located in near-fault areas, this study aims to investigate the following two effects in FP bearings: friction variability, as a function sliding velocity; friction force and restoring stiffness during the sliding phase, proportional to the axial load variation. To this end, a six-storey reinforced concrete (r.c.) framed building, characterized by an L-shaped plan with wings of different length and setbacks at different heights along the in-plan X (i.e. one setback, at the third-storey) and Y (i.e. two setbacks, at the second- and fourth-storey) principal directions is considered. In detail, twelve base-isolated structures are designed in line with the Italian seismic code (NTC08, [13]), with the horizontal seismic loads acting alone or in combination with the vertical ones. Furthermore, two in-plan distributions of low-type friction properties, ranging from a constant value for all isolators to a different value for each, are designed for three low-to-medium design values of the radius of curvature of the FP bearings. Two sets of seven near-fault earthquakes, each with significant components in the horizontal or vertical direction, are selected from the *Pacific Earthquake Engineering Research center database* (PEER, [14]) and normalized with the design hypotheses adopted for the test structure (i.e. medium-risk seismic region and stiff site).

2 LAYOUT AND DESIGN OF THE BASE-ISOLATED BUILDINGS

A six-storey r.c. office building base-isolated with the FP system, characterized by an L-shaped plan with wings of different length (Figure 1a) and setbacks at different heights (Figure 1b), is considered as test structure. It is designed in line with NTC08 [13] and besides the gravity loads, the horizontal seismic loads are assumed to act alone or in combination with the vertical ones. The following design assumptions are considered: elastic response of the superstructure (i.e. behaviour factor for the horizontal seismic loads, q_H=1; behaviour factor for the vertical seismic loads, q_V=1); stiff site (i.e. subsoil class B); medium-risk seismic region (i.e. peak ground accelerations: $PGA_{H,LS}$=0.16gx1.2=0.19g and $PGA_{V,LS}$= 0.08g, at the life-safety limit state for the superstructure; $PGA_{H,CP}$=0.21gx1.2=0.25g and $PGA_{V,CP}$=0.13g, at the collapse prevention limit state for the base-isolation system). The gravity loads used in the design are represented by a dead load of 6.7 kN/m^2 and a live load of 2.0 kN/m^2, on all floors, and a perimeter masonry-infills of 2.7 kN/m^2, on the first five floors. A cylindrical compressive strength of 25 N/mm^2 for the concrete and a yield strength of 450 N/mm^2 for the steel are assumed for the r.c. frame members, whose cross sections are reported in Tables 1 and 2.

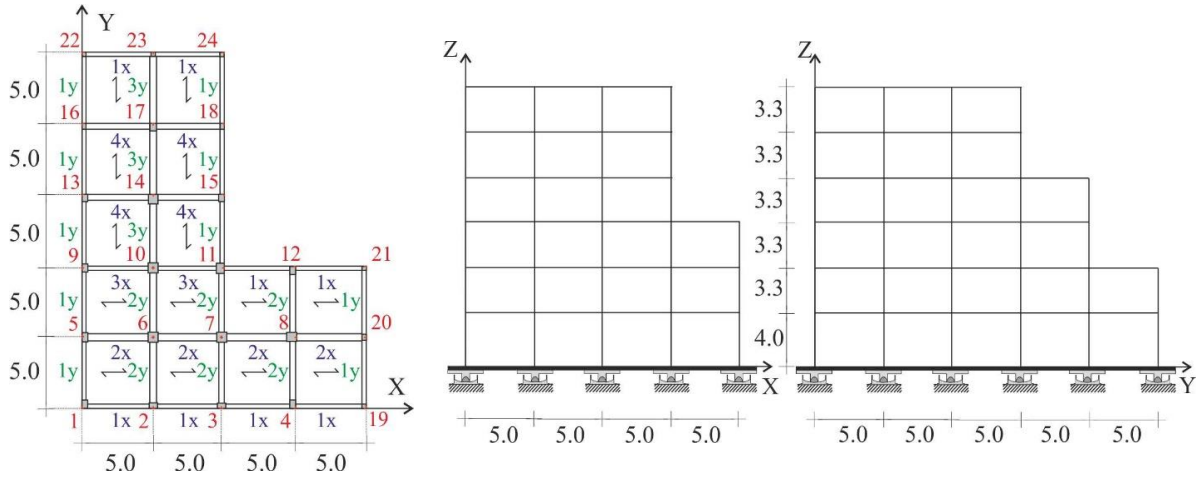

(a) Plan. (b) Elevations.

Figure 1: Base-isolated test structure (units in m).

	Floor level					
Beam	1	2	3	4	5	6
1x	30×60	30×60	30×60	30×60	30×60	30×60
2x	50×21	50×21	50×21	50×21	50×21	50×21
3x	30×55	30×55	30×55	30×55	30×55	30×55
4x	40×65	40×65	40×65	40×65	-	-
1y	30×60	30×60	30×60	30×60	30×60	30×60
2y	40×65	40×65	40×65	40×65	40×65	40×65
3y	50×21	50×21	50×21	50×21	50×21	50×21

Table 1: Cross-sections of r.c. beams (units in cm).

	Storey					
Column	1	2	3	4	5	6
1	40×60	35×55	30×50	30×45	30×40	30×35
2	60×40	50×35	50×30	40×30	30×30	30×30
3	60×40	50×35	50×30	40×30	30×30	30×30
4	40×60	35×55	30×50	30×45	30×40	30×35
5	40×60	35×50	35×40	30×40	30×30	30×30
6	70×70	65×65	60×60	50×50	40×40	30×30
7	70×70	65×65	60×60	50×50	40×40	30×30
8	60×60	55×55	50×50	45×40	40×30	35×30
9	40×60	35×50	30×50	30×40	30×30	30×30
10	70×70	65×65	60×60	50×50	40×40	30×30
11	55×70	50×65	45×60	40×50	35×40	30×30
12	40×60	35×55	30×50	30×45	30×40	30×35
13	40×50	35×50	30×40	30×35	30×30	30×30
14	65×65	60×60	50×50	45×45	35×40	30×35
15	40×50	35×45	30×40	30×35	30×30	30×30
16	30×40	30×35	30×30	30×30	-	-
17	50×50	45×45	35×40	30×35	-	-
18	30×40	30×35	30×30	30×30	-	-
19	30×30	30×30	30×30	-	-	-
20	30×40	30×35	30×30	-	-	-
21	30×30	30×30	30×30	-	-	-
22	30×30	30×30	-	-	-	-
23	35×30	30×30	-	-	-	-
24	30×30	30×30	-	-	-	-

Table 2: Cross-sections of r.c. columns (units in cm).

The FP system is designed at the CP limit state, requiring the fulfilment of the provisions imposed by NTC08: i.e. maximum compression axial load of the FP bearing less than its capacity; maximum horizontal displacements less than the spectral value; absence of tensile axial loads at the level of the FP system.

Three values of the effective fundamental vibration period of the isolation system

$$T_{e,I} = 2\pi \sqrt{\frac{1}{g\left(\frac{1}{R} + \frac{\mu_{fast}}{u_{H,d}}\right)}} \tag{1}$$

are considered (i.e.=2s, 2.5s and 3s), corresponding to the effective stiffness

$$K_e = N_{Sd}\left(\frac{1}{R} + \frac{\mu_{fast}}{u_{H,d}}\right) \tag{2}$$

and a value equal to 20% for the effective equivalent viscous damping

$$\xi_{e,I} = \frac{2}{\pi}\frac{1}{1+\frac{u_{H,d}}{\mu_{fast}R}} \tag{3}$$

The nonlinear system based on Equations (1) and (3) returns the values of the radius of curvature (R) and dynamic-fast friction coefficient (μ_{fast}) of the FP bearings, which correspond to the spectral displacement ($u_{H,d}$). Then, the maximum axial load capacity of the FP bearings (N_{Ed}) is evaluated by Equations (4a) and (4b), as function of the assigned value of the quasi-permanent gravity loads (N_{Sd}) transmitted from the superstructure [15]

$$\mu_{fast}(\%) = 17, \quad \left(\frac{N_{Sd}}{N_{Ed}}\right) \le 0.1 \tag{4a}$$

$$\mu_{fast}(\%) = 2.5\left(\frac{N_{Sd}}{N_{Ed}}\right)^{-0.834}, \quad \left(\frac{N_{Sd}}{N_{Ed}}\right) > 0.1 \tag{4b}$$

Moreover, two in-plan distributions of N_{Ed} are assumed for the FP bearings: case A in Figure 2a, with fifteen types of FP bearings (i.e. μ_{fast} equal for all isolators); case B in Figure 2b, with only three types of FP bearings (i.e. μ_{fast} different for each isolator), which are selected with reference to the maximum value of N_{Ed} from those of the isolators corresponding to three ranges of $\beta=N_{Sd}/N_{Sd,max}$ (i.e. $\beta\le0.4$; $0.4<\beta\le0.7$; $\beta>0.7$). It is worth noting that the final values of μ_{fast} take into account the fact that the FP bearings need the fulfilment of the CP limit state imposed by NTC08. For all the examined cases, design parameters of the FP systems are reported in Tables 3 and 4 where horizontal seismic loads act alone (i.e. H) or in combination with the vertical ones (i.e. HV), respectively.

	BI.AH1	BI.AH2	BI.AH3	BI.BH1	BI.BH2	BI.BH3
T_{eI} (s)	1.95	2.33	2.62	1.97	2.33	2.61
ξ_{eI} (%)	22.0	25.8	30.2	21.0	25.3	30.2
R (m)	1.45	2.26	3.26	1.45	2.26	3.26

Table 3: Dynamic and geometric parameters of Friction Pendulum (FP) systems designed for horizontal seismic loads.

	BI.AHV1	BI.AHV2	BI.AHV3	BI.BHV1	BI.BHV2	BI.BHV3
T_{el} (s)	1.90	2.21	2.49	1.95	2.26	2.54
ξ_{el} (%)	24.0	29.3	33.5	22.0	27.4	32.0
R (m)	1.45	2.26	3.26	1.45	2.26	3.26

Table 4: Dynamic and geometric parameters of Friction Pendulum (FP) systems designed for horizontal and vertical seismic loads.

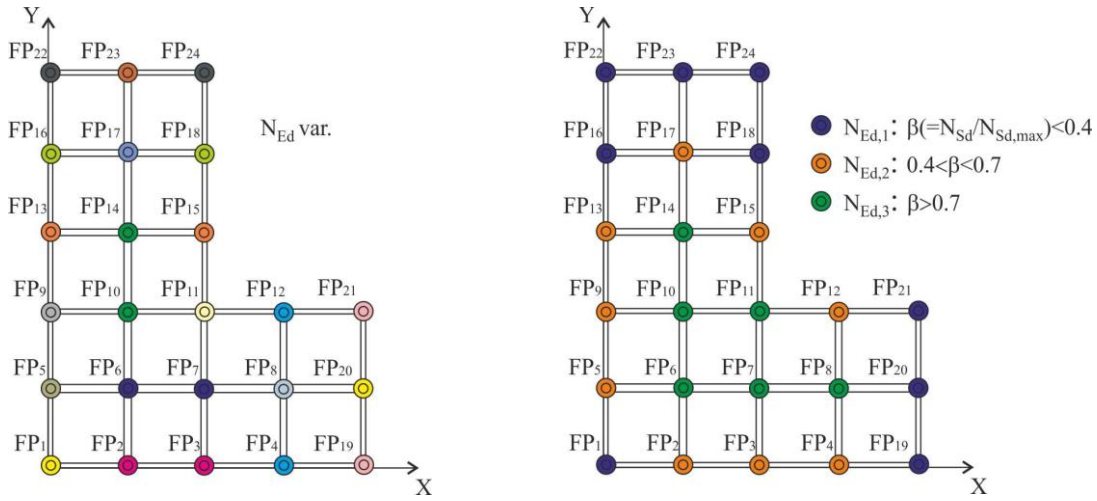

(a) BI.A structures: n.15 FP. (b) BI.B structures: n.3 FP.

Figure 2: In-plan distributions of axial load capacity for the Friction Pendulum (FP) bearings.

3 NONLINEAR MODELLING OF THE FP BEARINGS

The single FP bearing consists of a spherical concave sliding surface of polished stainless steel, with a radius of curvature R and a centre of curvature C, and an articulated slider coated with a layer of low friction composite material. The frictional force and stiffness during the sliding phase are proportional to the axial load. Moreover, an exponential analytical law can describe the velocity dependence of the dynamic friction coefficient [16]

$$\mu = \mu_{fast} - \left(\mu_{fast} - \mu_{slow}\right) e^{-\alpha \dot{u}_H} \tag{5}$$

where μ_{fast} and μ_{slow} are the friction coefficients at fast and slow sliding velocities $\dot{u}_H$, respectively, and α is a rate parameter which depends on the contact pressure and condition of the interface. The experimental results indicate that μ_{slow} can be assumed to be 2.5 times lower than μ_{fast} [17], while α can be considered approximately equal to 0.0055 s/mm [18].

The friction force for horizontal (bidirectional) motion is equal to [19]

$$\boldsymbol{F}_f = \begin{Bmatrix} F_{f,x} \\ F_{f,y} \end{Bmatrix} \cong \mu N \frac{1}{\|\dot{\boldsymbol{u}}_H\|} \begin{Bmatrix} \dot{u}_{H,x} \\ \dot{u}_{H,y} \end{Bmatrix} \tag{6}$$

where N is the axial load on the FP bearing. Finally, the restoring force can be evaluated as [20]

$$\boldsymbol{F}_H = \begin{Bmatrix} F_{H,x} \\ F_{H,y} \end{Bmatrix} \cong \frac{N}{R} \begin{Bmatrix} u_{H,x} \\ u_{H,y} \end{Bmatrix} + \begin{Bmatrix} F_{f,x} \\ F_{f,y} \end{Bmatrix} \tag{7}$$

containing a pendular component, directed toward the centre of the bearing, and a friction component, acting in the opposite direction to the velocity. For constant values of axial load and friction coefficient, the force-displacement behaviour of the FP bearing in the horizontal

direction (F_H-u_H) can be idealized by a bilinear law with lateral restoring stiffness

$$K_r = \frac{N}{R} \tag{8}$$

However, due to high values of vertical ground acceleration and global overturning moment produced by the horizontal seismic loads, the axial load variation on the FP bearing leads to changes in μ, F_f and K_r. In particular, at any given moment during an earthquake, the weight (W) of the superstructure acting on a FP bearing can be modified in accordance with the following expression [9]

$$N = W\left(1 - \frac{\ddot{u}_{g,V}}{g} + \frac{N_{OM}}{W}\right) \tag{9}$$

where $\ddot{u}_{g,V}$ is the vertical ground acceleration (positive when the direction is downwards) and N_{OM} is the additional axial load due to overturning (positive when compressive). It is worth noting that the fluctuation in the bearing axial load can be large enough to produce reversal of the axial load from compression to tension. A gap element is considered in the vertical direction, to take into account the fact that the FP bearing does not resist tensile axial loads and thus is free to uplift, assuming infinite rigidity in compression.

Maximum floor rotation at the level of the FP system, during the total duration (t_{tot}) of each ground motion, is evaluated as

$$\tan\vartheta_{max} = \max\left\{\left|u_{X,1}(t) - u_{X,22}(t)/L_Y\right| = \left|u_{Y,1}(t) - u_{Y,19}(t)/L_X\right|\right\},\ t\text{=0-}t_{tot} \tag{10}$$

referring to the horizontal displacement of three FP bearings at the corners of the building plan (i.e. FP_i, i=1, 19 and 22 in Figure 1a), being L_X=20m and L_Y=25m the maximum length along the X and Y directions. Moreover, the maximum residual displacement of the FP bearings is obtained as the vector sum of the residual displacement along the local axes

$$u_{res,max} = \max\left\{\sqrt{(u_{resx,i})^2 + (u_{resy,i})^2 + (u_{resz,i})^2}\right\},\ \text{i=1-24} \tag{11}$$

while the maximum vertical uplift

$$u_{up,max} = \max\left\{\left|u_{V,i}(t) - R\left[1 - cos\left(arcsin\frac{u_{H,i}(t)}{R}\right)\right]\right|\right\},\ \text{i=1-24} \tag{12}$$

is obtained as function of vertical and horizontal displacements on their spherical surface.

4 UNSCALED AND SCALED NEAR-FAULT GROUND MOTIONS

Ground motions recorded at near-fault sites may be characterized by strong long-duration velocity pulses in the horizontal direction, which may affect the friction coefficient of the FP bearings and their axial load variation due to overturning. To study torsional and re-centring problems of base-isolated structures with the FP system subjected to near-fault ground motions, seven recordings with significant horizontal components are selected from the *Pacific Earthquake Engineering Research center database* [14] on the basis of the design hypotheses adopted for the test structures. In Table 5a their main data are shown: i.e. year; recording station; closest distance from the fault (Δ); magnitude (M_w); peak ground acceleration for the two horizontal (i.e. PGA_{H1} and PGA_{H2}) and the vertical component (i.e. PGA_V); orientation of the strongest observed pulse (α_{sp}), clockwise from North [21].

Earthquake (EQ)	Station	Δ (km)	M_w	$PGA_{H,1}$	$PGA_{H,2}$	PGA_V	α_{sp}
Chi-Chi, 1999	TCU068	0.3	7.6	0.566g	0.462g	0.486g	144°
Imperial Valley, 1979	El Centro D.A.	5.1	6.5	0.353g	0.481g	0.770g	253°
Kobe, 1995	Takatori	1.5	6.9	0.618g	0.671g	0.284g	318°
Loma Prieta, 1989	Gilroy A#3	12.8	6.9	0.559g	0.368g	0.342g	277°
Northridge, 1994	Rinaldi R.S.	6.5	6.7	0.874g	0.472g	0.958g	209°
Parkfield, 2004	Fault Zone 1	2.5	6.0	0.605g	0.833g	0.255g	13°
Superstition Hills, 1987	Parachute T.S.	1.0	6.5	0.432g	0.384g	-	242°

Table 5a: Characteristics of the selected near-fault ground motions with significant horizontal components.

On the other hand, near-fault ground motions may be characterized by high values of the acceleration ratio $\alpha_{PGA}(=PGA_V/PGA_H)$, which may influence the friction force and lateral stiffness of the FP bearings during the sliding phase and produce uplift of the FP bearings. To study the nonlinear response of base-isolated structures with the FP system subjected to near-fault ground motions with significant vertical component, seven recordings are selected from the *PEER database*. Table 5b shows their main data: i.e. year; recording station; closest distance from the fault (Δ); magnitude (M_w); peak ground accelerations (i.e. PGA_{H1}, PGA_{H2} and PGA_V); maximum value of the acceleration ratio (i.e. $\alpha_{PGA,max}$).

Earthquake (EQ)	Station	Δ (km)	M_w	$PGA_{H,1}$	$PGA_{H,2}$	PGA_V	$\alpha_{PGA,max}$
Nahanni, 1985	Station I	6.0	6.76	1.108g	1.201g	2.281g	2.059
Imperial Valley, 1979	El Centro D.A.	5.1	6.50	0.353g	0.481g	0.770g	2.181
Imperial Valley, 1979	El Centro A#7	0.6	6.50	0.341g	0.469g	0.579g	1.698
Morgan Hill, 1984	Gilroy A#3	10.3	6.19	0.195g	0.201g	0.403g	2.067
Coyote Lake. 1979	Gilroy A#4	5.7	5.70	0.233g	0.252g	0.422g	1.811
Whittier Narrows, 1987	Arcadia Campus	17.4	5.9	0.293g	0.176g	0.223g	1.267
Westmorland, 1981	Westmorland F.S.	6.5	5.9	0.377g	0.498g	0.812g	2.154

Table 5b: Characteristics of the selected near-fault ground motions with significant vertical component.

To account for the potential structural damage of near-fault earthquakes, maximum value of spectral acceleration is assumed as a seismic intensity measure. In detail, horizontal components corresponding to the effective fundamental vibration period (i.e. T_{eI}) and equivalent viscous damping (i.e. ξ_{eI}) of the base-isolated structures reported in Tables 3 and 4 (i.e. $S^{(NF)}{}_{aH,1}$ and $S^{(NF)}{}_{aH,2}$) are considered. Then, the scale factor (*SF*), whereby the selected accelerograms are normalized with respect to the NTC08 spectrum, is evaluated as

$$SF = \frac{S_{aH}^{NTC08}\left(T_{eI},\xi_{eI}\right)}{\max\left\{S_{aH,1}^{NF}\left(T_{eI},\xi_{eI}\right),S_{aH,2}^{NF}\left(T_{eI},\xi_{eI}\right)\right\}} \tag{13}$$

Finally, normalization of the selected near-fault ground motions is carried out by scaling their *PGA* values with reference to *SF* values reported in Tables 6a and 6b.

	SF					
Earthquake (EQ)	BI.AH1	BI.AH2	BI.AH3	BI.BH1	BI.BH2	BI.BH3
Chi-Chi, 1999	0.28	0.25	0.21	0.28	0.25	0.21
Imperial Valley, 1979	0.64	0.52	0.47	0.64	0.52	0.47
Kobe, 1995	0.17	0.22	0.28	0.17	0.22	0.27
Loma Prieta, 1989	0.61	0.62	0.62	0.62	0.62	0.62
Northridge, 1994	0.27	0.32	0.32	0.27	0.32	0.32
Parkfield, 2004	0.59	0.75	0.82	0.60	0.75	0.82
Superstition Hills, 1987	0.21	0.23	0.22	0.21	0.23	0.22

Table 6a: Scale factors of the selected near-fault ground motions with significant horizontal components.

	SF					
Earthquake (EQ)	BI.AHV1	BI.AHV2	BI.AHV3	BI.BHV1	BI.BHV2	BI.BHV3
Nahanni, 1985	1.08	1.05	1.04	1.07	1.11	1.04
Imperial Valley, 1979	0.67	0.54	0.50	0.64	0.53	0.49
Imperial Valley, 1979	0.37	0.34	0.32	0.36	0.34	0.32
Morgan Hill, 1984	2.06	2.33	2.16	2.04	2.32	2.12
Coyote Lake. 1979	1.64	1.89	2.14	1.70	1.94	2.15
Whittier Narrows, 1987	3.08	3.24	3.30	3.22	3.26	3.27
Westmorland, 1981	0.69	0.89	1.00	0.71	0.94	1.02

Table 6b: Scale factors of the selected near-fault ground motions with significant vertical component.

5 NUMERICAL RESULTS

A numerical study is carried out to analyze torsional response, re-centring capability and uplift of base-isolated structures subjected to near-fault ground motions. In detail, maximum effects are evaluated for the orientation of the strongest pulse (i.e. $\alpha=\alpha_{sp}$) in the case of earthquakes with significant horizontal components, while accelerograms applied in line with the direction of the recording station (i.e. $\alpha=\alpha_{rs}$) are considered for earthquakes with significant vertical component. A computer code is adopted for the nonlinear dynamic analysis of the test structures [22-25], considering an elastic-linear behaviour of the superstructure and a nonlinear force-displacement law of the FP bearings in the horizontal direction depending on sliding velocity and axial load. A gap model is also assumed to capture the uplift of the FP bearings in the vertical direction. Moreover, a stiffness-proportional damping matrix of the superstructure is considered, by applying a viscous damping ratio ξ_S=1% to the fundamental vibration period of the base-isolated structures [26]. To take into account the uncertainty in the selection of the seismic intensity measure [27] and code-mandated damping modification factor [28] to be adopted for base-isolated structures subjected to near-fault earthquakes, two series of analyses are carried out on the selected ground motions applied with and without the scaling factor described in Section 4.

Firstly, maximum values of floor rotation ($tan\theta_{max}$) and residual displacement ($u_{res,max}$) at the level of the FP system are reported in Figures 3a-4a and 3b-4b, respectively, for base-isolated structures subjected to the unscaled Chi-Chi and Nahanni near-fault earthquakes (EQs). Two in-plan distributions of dynamic-fast friction coefficient for the FP system (i.e. BI.A and BI.B structures) are compared for three low-to-medium values of the radius of curvature for the FP bearings (i.e. R=1.45m, 2.26m and 3.26m).

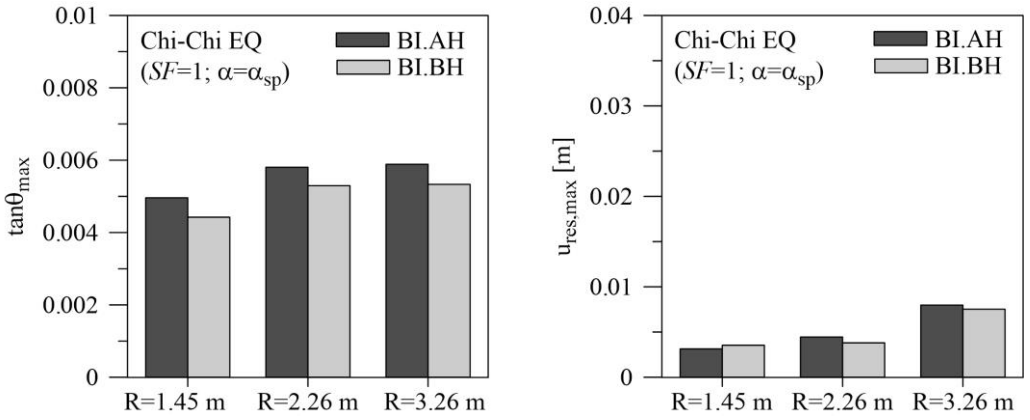

(a) Floor rotation. (b) Residual displacement.

Figure 3: Effects of the radius of curvature of the FP bearings on the nonlinear response of base-isolated structures subjected to the unscaled Chi-Chi EQ.

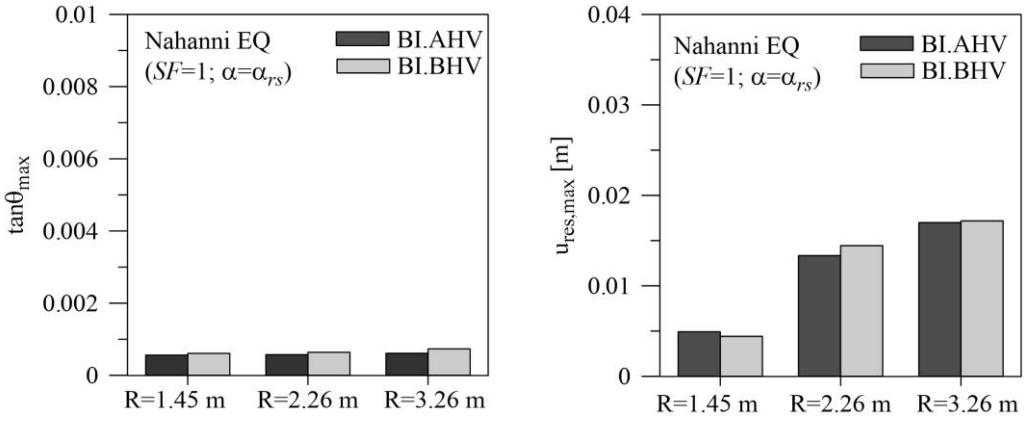

(a) Floor rotation. (b) Residual displacement.

Figure 4: Effects of the radius of curvature of the FP bearings on the nonlinear response of base-isolated structures subjected to the unscaled Nahanni EQ.

The BI.AH and BI.BH structures are designed considering the horizontal seismic loads acting alone and thus they are subjected to the Chi-Chi EQ (Figure 3), in which significant horizontal components are dominant; on the other hand, the Nahanni EQ (Figure 4), with a significant vertical component, is considered for the BI.AHV and BI.BHV structures designed also considering the vertical seismic loads. As can be noted, torsional effects are found to be important for the Chi-Chi EQ (Figure 3a), while in the case of the Nahanni EQ the effect is minor (Figure 4a). On the other hand, the residual displacement is generally more marked for the base-isolated structures subjected to the Nahanni EQ (Figure 4b) than the Chi-Chi EQ (Figure 3b). This behaviour can be interpreted by observing that higher spectral values of acceleration in the vertical direction are obtained for the Nahanni EQ, at least for rather low values of the vibration periods, thereby increasing the friction threshold of the FP bearings. As expected, the concave spherical surface of the FP bearing ensures a reduction of the residual displacement for decreasing values of the radius of curvature (Figures 3b and 4b). The BI.BH and BI.BHV structures respond in a similar way to the corresponding BI.AH and BI.AHV structures, but the former are less expensive because they require only three typologies of isolators in accordance with the maximum axial load capacity of the FP bearings.

Similar graphs in Figure 5 refer to minimum and maximum percentage of re-centring displacement ($u_{rec,\%}$) compared to maximum horizontal displacement.

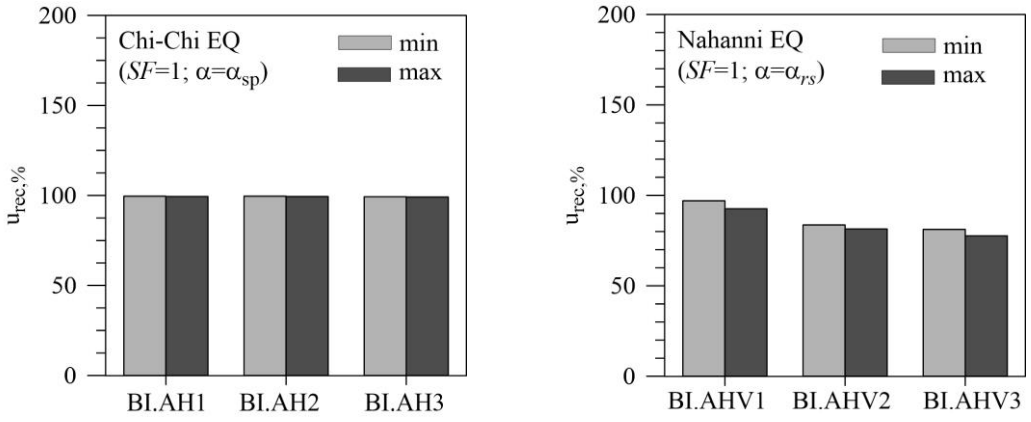

(a) (b)

Figure 5: Percentage of re-centring displacement for base-isolated structures subjected to the unscaled Chi-Chi and Nahanni EQs.

The BI.AHV structures subjected to the unscaled Nahanni EQ (Figure 5b) highlight values of $u_{rec,\%}$ lower than those obtained for the BI.AH structures under the Chi-Chi EQ (Figure 5a). Moreover, it is worth noting that the BI.AHV structures subjected to the Nahanni EQ exhibit different minimum and maximum values of $u_{rec,\%}$, highlighting the possibility of residual floor rotation at the level of the FP system.

Next, maximum values of uplift ($u_{up,max}$) for the BI.AHV and BI.BHV structures subjected to the unscaled Nahanni EQ are compared in Figure 6. More specifically, uplift of the six FP bearings at the corners of the building plan (i.e. FP_i, i=1, 11, 19, 21, 22 and 24 shown in Figure 1a) are reported. Note that uplift takes place in all the examined cases although the presence of tensile axial loads at the level of the FP system was prevented when designed for the horizontal seismic loads acting in combination with the vertical seismic ones. As can be observed, the variability of the in-plan distribution of friction coefficient and the choice of different radii of curvature for the FP bearings are not able to prevent uplift. Further results, omitted for brevity, confirm the absence of uplift due to overturning produced by the horizontal components of the unscaled Chi-Chi EQ.

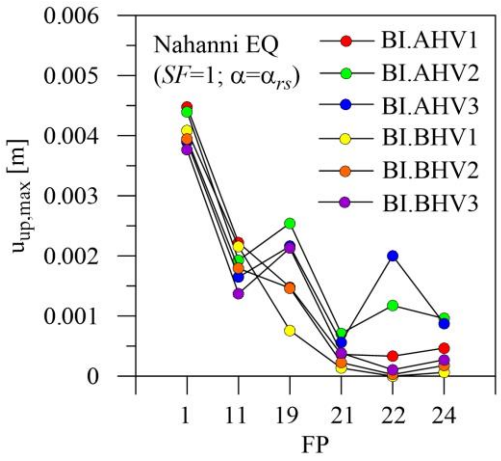

Figure 6: Effects of the radius of curvature of the FP bearings on the uplift of base-isolated structures subjected to the unscaled Nahanni EQ.

Afterwards, in order to evaluate the effects of the modelling assumptions related to velocity dependence of the friction coefficient of the FP bearings, maximum values of the floor rotation and residual displacement are reported in Figures 7 and 8.

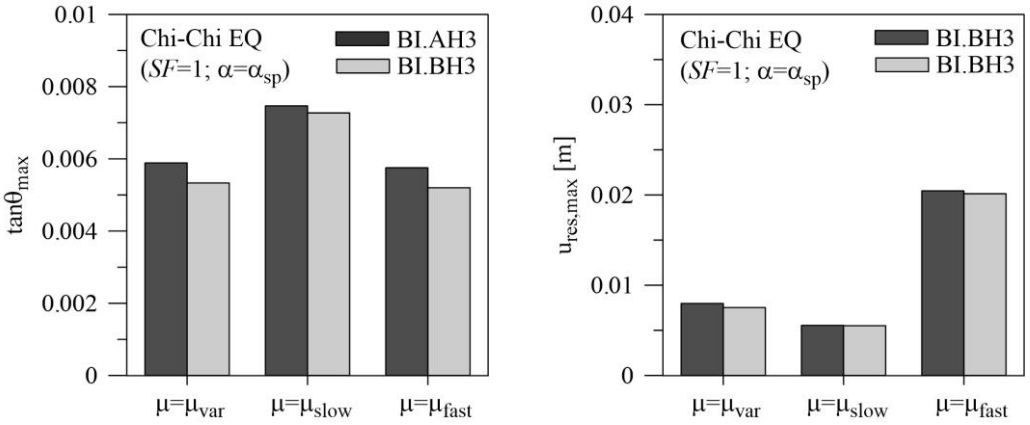

(a) Floor rotation. (b) Residual displacement.

Figure 7: Effects of modelling of the friction coefficient on the nonlinear response of base-isolated structures subjected to the unscaled Chi-Chi EQ.

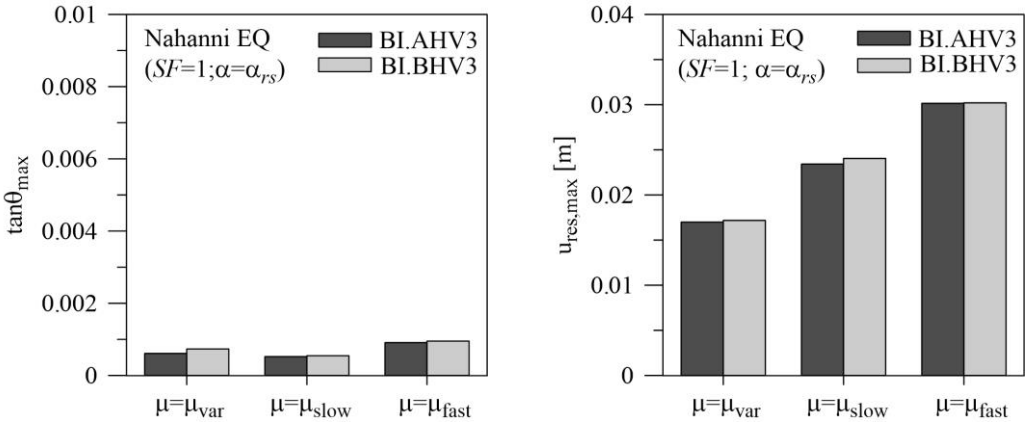

(a) Floor rotation. (b) Residual displacement.

Figure 8: Effects of modelling of the friction coefficient on the nonlinear response of base-isolated structures subjected to the unscaled Nahanni EQ.

Only results for base-isolated structures exhibiting maximum effects are examined for the unscaled Chi-Chi (i.e. BI.AH3 and BI.BH3 structures) and Nahanni (i.e. BI.AHV3 and BI.BHV3 structures) EQs. Three cases are compared: (a) friction coefficient variability as a function of the sliding velocity (i.e. $\mu=\mu_{var}$); (b) constant friction coefficient, at fast sliding velocity (i.e. $\mu=\mu_{fast}$); (c) constant friction coefficient, at slow sliding velocity (i.e. $\mu=\mu_{slow}$). As can be observed, maximum floor rotation is obtained for the BI.AH3 and BI.BH3 structures subjected to the Chi-Chi EQ (Figure 7a). This is evident when the minimum friction coefficient is assumed (i.e. μ_{slow}), while comparable results are found for the maximum (i.e. μ_{fast}) and variable (i.e. μ_{var}) friction coefficients. On the other hand, maximum values of residual displacement are obtained for the BI.AHV3 and BI.BHV3 structures under the Nahanni EQ (Figure 8b) and correspond to maximum friction coefficient (μ_{fast}); lower values are obtained for the minimum (μ_{slow}) and variable (μ_{var}) friction coefficients. In all the examined cases, comparable results are obtained for the base-isolated structures designed to consider the two in-plan distributions of the FP bearings (i.e. cases A and B shown in Figure 2).

Finally, maximum ($tan\theta_{max}$) and mean ($tan\theta_{mean}$) floor rotations along the building height are plotted for base-isolated structures subjected to two sets of seven scaled near-fault ground motions with significant horizontal (Figure 9) and vertical (Figure 10) components.

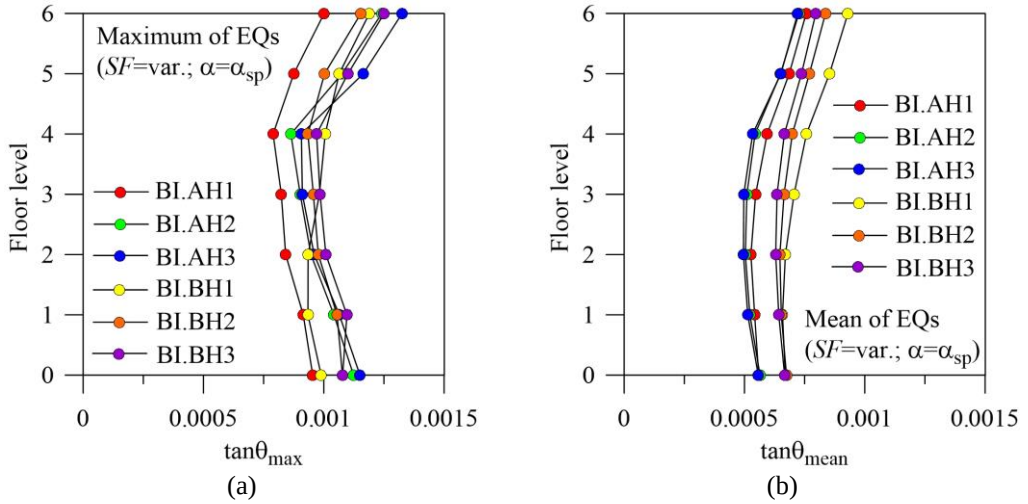

(a) (b)

Figure 9: Maximum and mean floor rotations of the superstructure for scaled near-fault EQs with significant horizontal components.

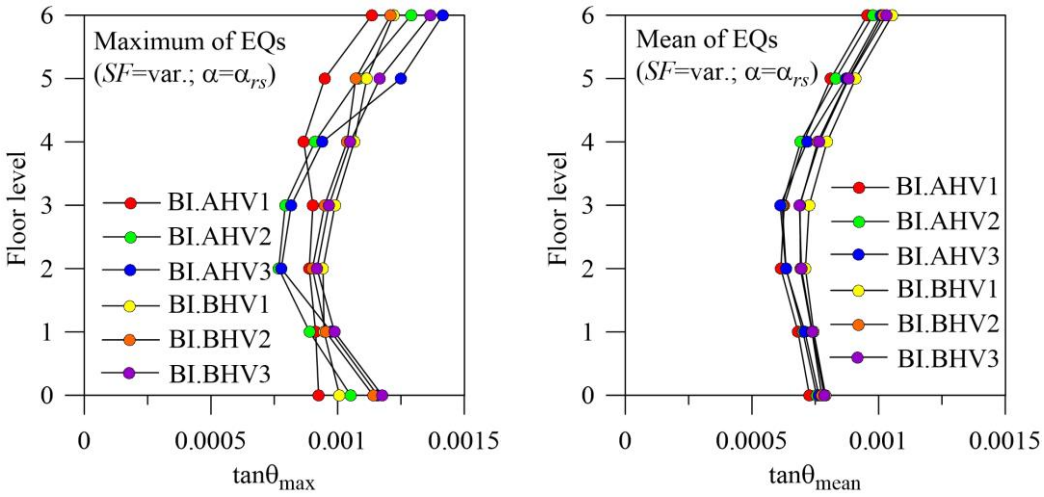

Figure 10: Maximum and mean floor rotations of the superstructure for scaled near-fault EQs with significant vertical component.

Note the highest values of floor rotation at the top level, with variability of torsional effects at the floor levels of the superstructure which are more evident in terms of $tan\theta_{max}$ (Figures 9a and 10a) than $tan\theta_{mean}$ (Figures 9b and 10b). However, limited torsional effects are highlighted for all the examined structures subjected to scaled near-fault EQs, which are normalized in accordance with a medium risk seismic region. Further results, omitted for the sake of brevity, highlight low values of maximum and mean residual displacement and uplift of the FP system.

6 CONCLUSIONS

The nonlinear seismic analysis of base-isolated structures with the FP system is carried out under near-fault ground motions, considering three low-to-medium design values of the radius of curvature of the FP bearings and two in-plan distributions of their dynamic-fast friction coefficient. Torsional effects are found to be more evident for unscaled earthquakes with significant horizontal components (e.g. the Chi-Chi EQ). On the other hand, residual displacement are generally more marked for base-isolated structures subjected to unscaled earthquakes with significant vertical component (e.g. the Nahanni EQ). Torsional and residual effects of the BI.BH and BI.BHV structures are similar to those of the corresponding BI.AH and BI.AHV structures, but the former are less expensive because they require only three typologies of isolators. As expected, a reduction of the residual displacement is obtained for decreasing values of the radius of curvature of the FP bearings. It is interesting to note that the BI.AHV structures subjected to the Nahanni EQ exhibit different minimum and maximum values of the percentage of re-centring displacement, highlighting the possibility of residual floor rotation at the level of the FP system. Moreover, the BI.AHV and BI.BHV structures exhibit uplift when subjected to the Nahanni EQ. The modelling of the friction coefficient highlights maximum floor rotation under the Chi-Chi EQ, when the minimum (constant) friction coefficient is assumed, while comparable results are found for maximum (constant) and variable friction coefficients. Maximum values of residual displacement are obtained under the Nahanni EQ, corresponding to maximum (constant) friction coefficient, while lower values are obtained for the minimum (constant) and variable friction coefficients. Finally, the highest values of mean floor rotation are found at the top level of the superstructure. However, torsional effect and residual displacement and uplift are less evident for scaled near-fault earthquakes, confirming the crucial importance of selecting suitable seismic intensity measure and code-mandated damping modification factor.

ACKNOWLEDGEMENTS

The present work was also financed by Re.L.U.I.S. (Italian network of university laboratories of earthquake engineering), in accordance with "Convenzione D.P.C.–Re.L.U.I.S. 2014–2016, WPI, Isolation and Dissipation".

REFERENCES

[1] L. Petti, F. Polichetti, B. Palazzo, Analysis of seismic performance of FPS base isolated structures subjected to near fault events. *International Journal of Engineering and Technology*, **5**(6), 5233-5240, 2014.

[2] V.A. Zayas, S.S. Low, S.A. Mahin, A simple pendulum technique for achieving seismic isolation. *Earthquake Spectra*, **6**, 317–333, 1990.

[3] R.S. Jangid, Optimum friction pendulum system for near-fault motions. Engineering Structures **27**(3), 349-359, 2005.

[4] J.D. Bray, A. Rodriguez-Marek, J.L. Gillie, Design ground motions near active faults. *Bulletin of the New Zealand Society for Earthquake Engineering*, **42**(1), 1-8, 2009.

[5] E. Chioccarelli, I. Iervolino, Near-source seismic demand and pulse-like records: A discussion for L'Aquila earthquake. *Earthquake Engineering and Structural Dynamics* **39**(9), 1039-1062, 2010.

[6] G.M. Calvi, P. Ceresa, C. Casarotti, D. Bolognini, F. Auricchio, Effects of axial force variation in the seismic response of bridges isolated with friction pendulum systems. *Journal of Earthquake Engineering*, **8**(1), 187-224, 2004.

[7] F. Mazza, A. Vulcano, M. Mazza, Nonlinear dynamic response of rc buildings with different base-isolation systems subjected to horizontal and vertical components of near-fault ground motions. *The Open Construction and Building Technology Journal*, **6**, 373-383, 2012.

[8] J.L. Almazan, J.C. De la Llera, J.A.Inaudi, Modelling aspects of structures isolated with the frictional pendulum system. *Earthquake Engineering and Structural Dynamics* **27**, 845-867, 1998.

[9] P.C Roussis, M.C. Constantinou, Uplift-restraining friction pendulum seismic isolation system. *Earthquake Engineering and Structural Dynamics*, **35**, 577–593, 2006.

[10] M, Rabiei, F. Khoshnoudian, Response of multistory friction pendulum base-isolated buildings including the vertical component of earthquakes. *Canadian Journal of Civil Engineering*, **38**, 1045-1059, 2011.

[11] A.J. Papazoglou, A.S. Elnashai, Analytical and field evidence of the damaging effect of vertical earthquake ground motion. *Earthquake Engineering and Structural Dynamics*, **25**, 1109-1137, 1996.

[12] P. Carydis, C.A. Castiglioni, E. Lekkas, I. Kostaki, N. Lebesis, A. Drei, The Emilia Romagna, May 2012 earthquake sequence: the influence of the vertical earthquake component and related geoscientific and engineering aspects. *Ingegneria Sismica*, **2-3**, 31-58, 2012.

[13] NTC08. Technical Regulations for the Constructions. Italian Ministry of the Infrastructures 2008.

[14] PEER, Pacific Earthquake Engineering Research center. Next Generation Attenuation (NGA) database 2008, http://peer.berkeley.edu/peer_ground_motion_database.

[15] FIP Industriale S.p.A. Catalogue S04: Curved Surface Sliders. Padova, 2013, http://www.fipindustriale.it.

[16] M.C. Constantinou, A. Mokha, A.M. Reinhorn, Teflon bearings in base isolation. II: modeling. *Journal of Structural Engineering*, **116**(2), 455–474, 1990.

[17] M. Dolce, D. Cardone, F. Croatto, Frictional behavior of steel-PTFE interfaces for seismic isolation. *Bulletin of Earthquake Engineering*, **3**, 75–99, 2005.

[18] D. Cardone, G. Gesualdi, P. Brancato, Restoring capability of friction pendulum seismic isolation systems. *Bulletin of Earthquake Engineering*, **13**(8), 2449-2480, 2015.

[19] K.L. Ryan, A.K. Chopra, Estimating the seismic displacement of friction pendulum isolators based on non-linear response history analysis. *Earthquake Engineering and Structural Dynamics*, **42**, 2321-2339, 2004.

[20] G. Mosqueda, A.S. Whittaker, G.L. Fenves, Characterization and modeling of friction pendulum bearings subjected to multiple components of excitation. *Journal of Structural Engineering*, **130**(3), 433-442, 2004.

[21] S. Shahi, J. Baker, Pulse Classifications from NGA West2 database, 2012, http://web.stanford.edu/~bakerjw/pulse_classification_v2/Pulse-like-records.html.

[22] F. Mazza, M. Mazza, Nonlinear modeling and analysis of R.C. framed buildings located in a near-fault area. *The Open Construction & Building Technology Journal*, **6**, 346-354, 2012.

[23] F. Mazza, Nonlinear incremental analysis of fire-damaged r.c. base-isolated structures subjected to near-fault ground motions. *Soil Dynamics and Earthquake Engineering*, **77**, 192-202, 2015.

[24] F. Mazza, Effects of near-fault vertical earthquakes on the nonlinear incremental response of r.c. base-isolated structures exposed to fire. *Bulletin of Earthquake Engineering*, **14**, 433–454, 2016.

[25] F. Mazza, F. Alesina, Effects of site condition in near-fault area on the nonlinear response of fire-damaged base-isolated structures. *Engineering* Structures, **111**, 297-311, 2016.

[26] D.R. Pant, A.C. Wijeyewickrema, M.A. ElGawady, Appropriate viscous damping for nonlinear time-history analysis of base-isolated reinforced concrete buildings. *Earthquake Engineering and Structural Dynamics*, **42**, 2321-2339, 2013.

[27] H. Ebrahimian, F. Jalayer, A. Lucchini, F. Mollaioli, G. Manfredi, Preliminary ranking of alternative scalar and vector intensity measures of ground shaking. *Bulletin of Earthquake Engineering*, **13**, 2805-2840, 2015.

[28] F. Mollaioli, L. Liberatore, A. Lucchini, Displacement damping modification factors for pulse-like and ordinary records. *Engineering Structures*, **78**, 17-27, 2014.